Article:
Kamsanam, W, Mao, X and Jaworski, AJ (2015) Development of experimental techniques for measurement of heat transfer rates in heat exchangers in oscillatory flows. Experimental Thermal and Fluid Science, 62. 202 - 215. ISSN 0894-1777

https://doi.org/10.1016/j.expthermflusci.2014.12.008

Manuscript submitted to **Experimental Thermal and Fluid Science**

Development of experimental techniques for measurement of heat transfer rates in heat exchangers in oscillatory flows

Wasan Kamsanam[1], Xiaoan Mao[2,*] and Artur J. Jaworski[2]

[1)] Department of Engineering, University of Leicester, Leicester LE1 7RH, United Kingdom

[2)] Faculty of Engineering, University of Leeds, Leeds LS2 9JT, United Kingdom

Abstract

Heat exchangers are important components of thermoacoustic devices. In oscillatory flow conditions, the flow and temperature fields around the heat exchangers can be quite complex, and may significantly affect heat transfer behaviour. As a result, one cannot directly apply the heat transfer correlations for steady flows to the design of heat exchangers for oscillatory flows. The fundamental knowledge of heat transfer in oscillatory flows, however, is still not well-established. The aim of the current work is to develop experimental apparatus and measurement techniques for the study of heat transfer in oscillatory flows. The heat transferred between two heat exchangers forming a couple was measured over a range of testing conditions. Three couples of finned-tube heat exchangers with different fin spacing were selected for the experiment. The main parameters considered were fin spacing, fin length, thermal penetration depth and gas displacement amplitude. Their effects on the heat exchanger performance were studied. The results were summarised and analysed in terms of heat transfer rate and dimensionless heat transfer coefficient: Colburn-j factor. In order to obtain the gas side heat transfer coefficient in oscillatory flows, the water side heat transfer coefficient is required. Thus, an experimental apparatus for unidirectional steady test was also developed and a calculation method to evaluate the heat transfer coefficient was demonstrated. The uncertainties associated with the measurement of heat transfer rate were also considered.

Keywords: Oscillatory flow; Heat exchanger; Heat transfer rate; Colburn-j factor; Thermoacoustics

[*] To whom correspondence should be made
Tel: +44(0) 113 343 4807, E-mail: x.mao@leeds.ac.uk (X. Mao)

1. Introduction and literature review

In thermoacoustic heat engines, heat as an input energy is supplied from a high temperature source through a hot heat exchanger and waste heat is rejected to a heat sink with low temperature. The presence of the imposed steep temperature gradient in a solid structure called a stack or a regenerator sandwiched between the two heat exchangers produces acoustic power. In thermoacoustic refrigerators, heat is removed from where desired via a cold heat exchanger, transported via a stack or regenerator by supplied acoustic power, and rejected to the heat sink in an ambient heat exchanger. A simple standing wave thermoacoustic refrigerator and a schematic of thermoacoustic effect are illustrated in Fig. 1. The main components in the device as shown in Fig. 1(a) are an acoustic driver, a stack and two heat exchangers placed in the resonator. The driver sets up a half-wavelength acoustic field. This induces an oscillation of fluid elements in the vicinity of the stack and the heat exchangers.

A thermodynamic process takes place as shown in Fig. 1(b) due to expansion and contraction of fluid elements during their displacement cycle. The gas parcel at its largest volume moves leftward while simultaneously experiencing compression. At the leftmost position, it rejects heat to the stack as its temperature is raised above that of the local surface. This results in a decrease of the gas parcel's temperature which is subjected to the thermal contraction under high pressure. When the parcel moves rightward, it experiences adiabatic expansion enlarging its volume and decreasing its temperature below that of the local surface. At the rightmost position, the irreversible heat transfer takes place from the stack plate to the gas parcel causing the expansion of gas parcel volume and the rise of its temperature to the initial condition. All gas parcels behave as a 'bucket brigade' resulting in absorbing heat $\dot{Q}_c$ at temperature T_c and rejecting heat $\dot{Q}_{amb}$ at temperature T_{amb}. For a standing wave thermoacoustic engine, the process can be described in similar manner as given above for the refrigerator. However, the direction of thermodynamic cycle would be reversed.

As indicated, thermal interaction between working fluid and heat exchangers is crucial for the performance of thermoacoustic devices. Experimental works have been carried out in order to study the heat transfer in oscillatory flow. Temperature profiles at the interface of heated solid surface and oscillating gas were observed by Bouvier et al. (2005). Surface heat flux was determined from the temperature profiles measured on a test section of circular tube. The heat transfer characteristics were analysed as a function of acoustic Reynolds number $(\mathrm{Re}_1 = \rho u_1 d / \mu)$. Here ρ, μ, d and u_1 are density, dynamic viscosity of working gas, internal diameter of the tube and velocity amplitude,

respectively. Mozurkewich (2001) carried out tests on simple heat exchanger configurations consisting of parallel tubes located transversely adjacent to the hot end of a thermoacoustic stack. The experimental results were presented in terms of dimensionless heat transfer coefficient ($NuPr^{-0.37}$) as a function of the acoustic Reynolds number (Re_1). It was found that the dimensionless heat transfer coefficient increased with the increase of Re_1. A correlation was also developed to predict the heat transfer coefficient in thermoacoustic heat exchangers.

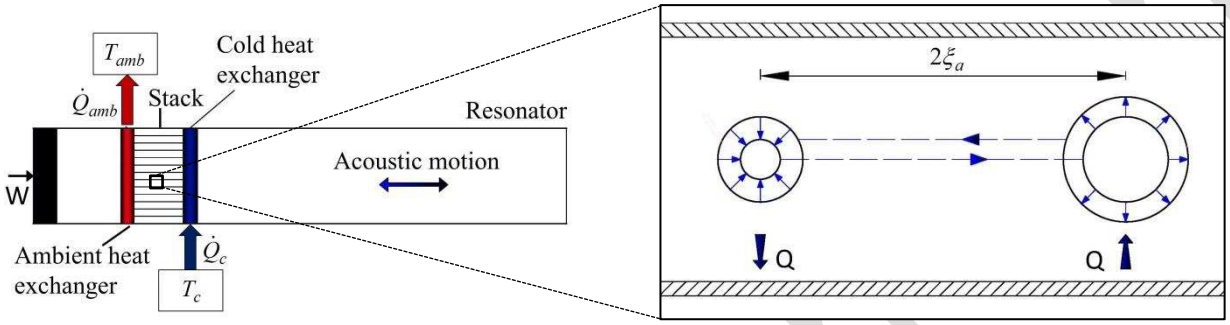

(a) (b)

Fig. 1. Standing wave thermoacoustic refrigerator (a), and a magnified view of thermoacoustic effect taking place in a channel of the stack (b).

Fabrication of heat exchangers used in thermoacoustic refrigerators was demonstrated by Garrett et al. (1994). Finned-tube heat exchangers were made and a simple derivation to evaluate their heat transfer performance was reported. Heat transfer coefficient was represented by root mean square value of the ratio of gas thermal conductivity and thermal penetration depth. Brewster et al. (1997) conducted an experimental measurement of the heat transfer coefficient for a parallel plate heat exchanger in a thermoacoustic refrigerator. The experimental results presented as a function of gas oscillation amplitude were also compared with developed models. Nsofor et al. (2007) and Tang et al. (2014) carried out experiments for oscillatory flow heat transfer from heat exchangers of thermoacoustic refrigerators. Both of these studies used parallel-plate heat exchangers but with different geometries. The parallel fins were attached to a cylindrical copper case having a channel where water could flow in its circumference. Based on the experimental results, Nsofor et al. (2007) developed a dimensionless heat transfer coefficient, Nusselt number (Nu), as a function of Prandtl number (Pr) and Reynolds number (Re) to predict the heat transfer performance. Tang et al. (2014) included also Valensi number $(Va = \rho\omega D_h^2 / \mu)$ in their proposed correlation. Here ω and D_h are angular frequency of flow oscillation and hydraulic diameter of fin spacing, respectively.

Wakeland and Keolian (2004) carried out measurements of heat transfer between two identical parallel plate heat exchangers (similar to car radiator) at various frequencies and gas displacement amplitudes. From the results, a correlation was proposed in the form of heat transfer effectiveness (the ratio of actual heat transfer rate to the maximum available heat transfer rate). A heat exchanger of a similar type was employed in an experiment by Paek et al. (2005) to evaluate oscillating flow heat transfer coefficient and to propose calculation methods. The experimental results were compared with existing models and a new correlation was presented.

The design of heat exchangers is a critical task in thermoacoustics, yet the knowledge of heat transfer in oscillatory flow conditions is limited. The relationship between heat transfer and heat exchanger geometry, as well as the operating conditions, needs to be investigated. In order to achieve the purpose, this study presents the development of an experimental apparatus in addition to the techniques to determine the heat transfer performance of heat exchangers in oscillatory flows. The dependence of the heat transfer rate and the dimensionless heat transfer coefficient, Colburn-j factor, on normalized displacement amplitude and normalized fin spacing for the heat exchangers under investigation is presented.

2. Experimental apparatus

A purpose-built oscillatory flow apparatus was designed and set up, as shown in Fig. 2. The working gas inside the stainless steel resonator pipe (2” diameter and 8.9 m long) is excited by a half wavelength standing wave created by the acoustic driver (Q-Drive, StarAlternator1S102M/A) installed on the left end. The other end of the resonator is closed. A couple of heat exchangers was installed in the test section, where the heat transfer between them was measured at various operating conditions.

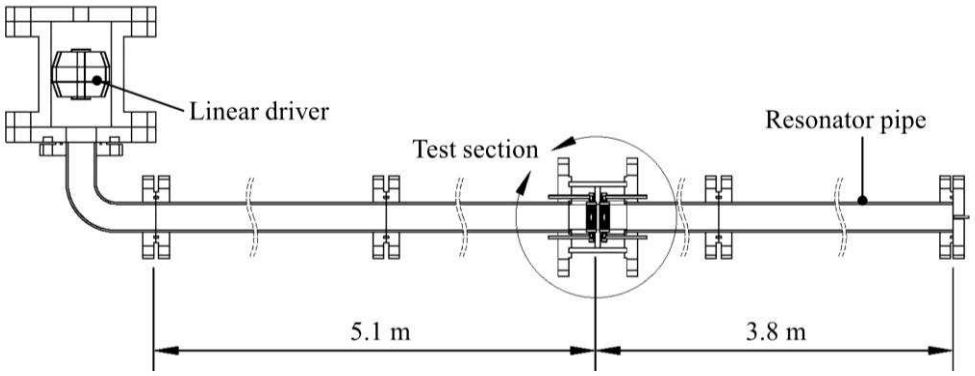

Fig. 2: A principle of the oscillatory flow experimental apparatus.

The working gas for the heat transfer in the oscillatory flow experiment was helium. The gas charging system consisted of a vacuum pump, valves, pressure gauges and a cylinder of pressurized helium gas, as shown in Fig. 3. Since the system may be operated at a high mean pressure of 33 bar, most parts were assembled with O-rings to prevent leakage. The displacement of the driver piston can be controlled to achieve the required excitation level. Operational parameters for controlling the linear driver, such as output voltage and frequency, could be selected. The driver has an excursion limit of 6 mm. A high-pressure window was installed in the driver housing for the access of a laser displacement sensor (Keyence model LK-G152) to monitor the piston displacement amplitude.

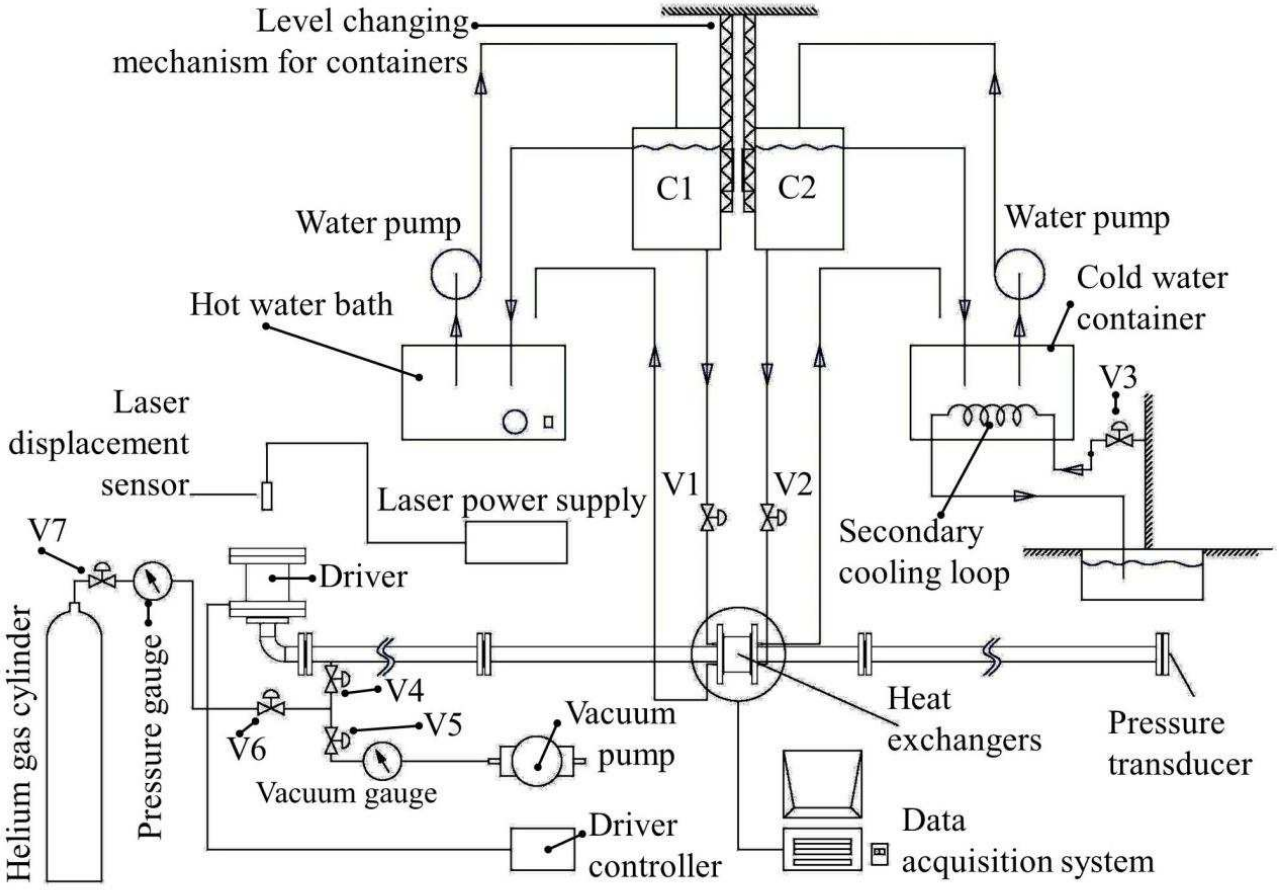

Fig. 3: Schematic diagram of the experimental apparatus for the oscillatory flow test.

Hot and cold water were the media used to deliver/extract heat to/from the hot and the cold side heat exchanger, respectively. The circulating loops for hot and cold water are shown in Fig. 3. The flow rate can be calculated from the mass of water collected within a period of time. Hot water is

pumped from the hot water bath with a maximum heating power of 1500 W and circulated through the hot heat exchanger. The water flow loop for the cold side heat exchanger was set up similar to the one on the hot side. The mass flow rate for hot and cold heat exchanger can be controlled through valves V1 and V2, respectively, or by changing the height of water containers. The temperature of the cooling water measured at the inlet of the cold side heat exchanger was maintained at 22 °C throughout the whole experiment. The secondary cooling flow loop was installed in the cold water bath to keep the water temperature steady. In the secondary cooling loop, cold water from a utility tap ran through a copper coil tube immersed in the cold water bath to carry heat to an external heat sink. The temperature in the cold-water bath was controlled by adjusting the flow rate of the cold water from the utility tap via valve V3 (see Fig. 3).

2.1 Test section

In the test section, two heat exchangers, one hot and another cold, were placed side by side. The stack or the regenerator normally found in a typical thermoacoustic engine or refrigerator was not present. This arrangement makes it possible to investigate the heat transfer from a heat exchanger to the oscillatory flow in a relatively wide range of flow conditions, without the concern of the operating mode of a thermoacoustic device being an engine or a refrigerator. The heat transfer analysis is carried out using the calorimetric method by measuring the heat transfer rate on the hot side heat exchanger, while the cold side heat exchanger is used to reject heat to the environment. The investigated combinations of hot and cold heat exchangers, as A, B and C, are shown in Table 1, where individual heat exchangers are labelled by HEX-n, 'n' being the heat exchanger number. The specification of heat exchangers is given in Section 2.2. A ceramic spacer was placed between them to provide a 5 mm distance (gap) between the heat exchanger faces. One heat exchanger performs as a hot heat exchanger and another as a cold heat exchanger. Heat transfer between them is measured and the influence of relevant parameters on the heat transfer is analysed. The test section is illustrated in Fig. 4.

Table 1: Hot and cold heat exchangers combinations

Combination	Fin spacing, D	
	Hot heat exchanger	Cold heat exchanger
A	HEX-1, D = 0.7 mm	HEX-1, D = 0.7 mm
B	HEX-2, D = 1.4 mm	HEX-3, D = 2.1 mm
C	HEX-3, D = 2.1 mm	HEX-2, D = 1.4 mm

In order to minimize heat loss to the outside, insulation was applied where possible. Silicate wool with a thermal conductivity of 0.1 $W \cdot m^{-1} \cdot K^{-1}$ was placed in the empty space between the heat exchanger and the stainless steel housing. The internal surfaces of the stainless steel pipe on both sides of the test section were covered by a polyethylene (PE) sheet with thermal conductivity of 0.5 $W \cdot m^{-1} \cdot K^{-1}$. The thickness of the PE sheet was 1.0 mm, which does not cause a significant obstruction to the gas flow. The length of the PE sheet measured from the flange surface into the pipe was about 10 cm; much longer than the maximum gas displacement amplitude in the experiment. A ceramic plate with thermal conductivity of 1.46 $W \cdot m^{-1} \cdot K^{-1}$ was used to separate two heat exchangers. It was introduced to reduce the heat conduction between hot and cold heat exchangers. Each heat exchanger was separated from the test section end-flanges using PTFE spacers – there is no direct contact between the copper heat exchanger case and the stainless steel flange. The thermal conductivity of the PTFE spacer is 0.25 $W \cdot m^{-1} \cdot K^{-1}$.

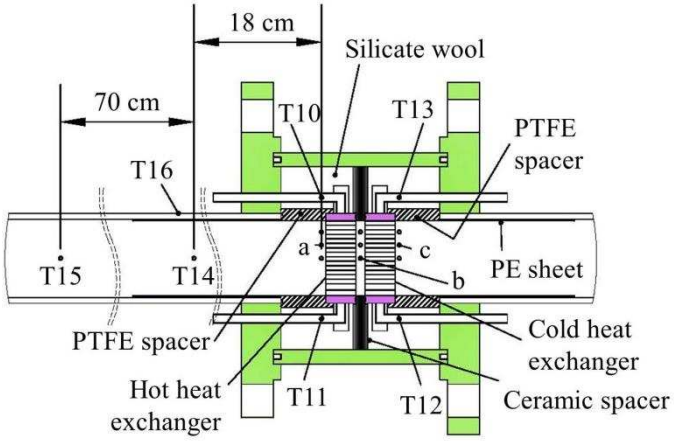

Fig. 4: A drawing of the test section in the oscillatory flow experiment.

2.2 Heat exchangers

The experiments were performed on heat exchangers with different fin spacings. The finned-tube type heat exchanger was selected for this study due to the simplicity of its construction, which in turn lowers the cost of fabrication. Heat exchanger specifications are detailed in Table 2. A photograph of assembled HEX-3 heat exchanger is shown in Fig. 5. Copper is the material used for making the finned-tube heat exchanger as it is an excellent thermal conductor. The mechanical strength was taken into account for the heat exchanger to operate in a pressurized environment.

Fig. 5: Finned-tube heat exchanger, HEX-3. The fin spacing is 2.1 mm.

In the fabrication process, heat exchanger components (fins, tubes, connectors and the heat exchanger case) are joined to form a complete heat exchanger unit. As the heat exchanger consists of many small fins to be fixed on copper tubes, they are joined by vacuum brazing technique. The oxygen-free copper C101 grade was selected.

Table 2: Heat exchanger specifications.

Parameters	Heat exchanger		
	HEX-1	HEX-2	HEX-3
Spacing between fins, D (mm)	0.7	1.4	2.1
Fin thickness, t (mm)	0.3	0.3	0.3
Fin length, L (mm)	20	20	20
Copper tube outer diameter, D_o (mm)	6	6	6
Copper tube inner diameter, D_i (mm)	5	5	5
Gas flow area (excluding copper pipes), A_{min} (mm^2)	830	950	1,015
Copper tube unfinned area, $A_{t,o}$ (mm^2)	1,742	2,111	2,217
Copper tube water side area, $A_{t,i}$ (mm^2)	2,090	2,090	2,090
Fin surface area, A_f (mm^2)	69,129	40,742	28,778
Gas side heat transfer area, A_o (mm^2)	70,871	42,853	30,995
Fin spacing hydraulic diameter, D_h (mm)	0.94	1.77	2.62
Heat exchanger porosity (σ)	0.64	0.75	0.79
Overall fin efficiency (η_0)	0.699	0.707	0.714

2.3 Measurement instrumentation

Thermocouple probes (Type K) were installed where necessary (Fig. 4) to take temperature readings for heat transfer analysis. The temperatures of the working gas facilitating the heat transfer calculation were collected from three locations; sections ‘a’, ‘b’ and ‘c’ as illustrated in Fig. 4. Section ‘b’ is located in the middle of the space between hot and cold heat exchangers to measure

the temperature of the oscillating gas in the gap. Sections ‘a’ and ‘c’ are located about 3 mm beside both heat exchangers. There are three thermocouple probes installed in each plane. Each probe is inserted into the test section chamber with different radial lengths. The water temperature readings at the inlet and exit of the hot and cold heat exchangers were achieved by probes T10, T11, T12 and T13. The temperature at the inlet of the hot heat exchanger (T10) was maintained at the desired level by using a PID controller. Two thermocouple probes, T14 and T15, were installed at 18 cm and 88 cm in front of the hot heat exchanger in order to observe the heat transfer by conduction through the working gas. The temperature reading of the stainless steel pipe on its external surface was obtained from a thermocouple probe T16, which was used to estimate the conductive heat transfer through the pipe wall. Temperature data obtained from all probes was collected by a data acquisition system, Omega OMB-DaqTemp. A Snowrex NE-15 digital scale with 0.5 g resolution was used to weigh the collected water. The elapsed time was obtained from a digital stopwatch. Acoustic pressure amplitude was measured by a PCB PIEZOTRONICS pressure transducer model 112A21, which was attached to the end of the resonator pipe.

2.4 Experimental apparatus for steady flow experiment

The heat transfer coefficient of water side (h_i) is required for the evaluation of heat transfer coefficient of gas side in oscillatory flow experiment ($h_{o,OSC}$). A separate arrangement for the measurement in a steady flow was also set up. More specifically, the steady flow refers to a unidirectional flow with a constant velocity, in contrast to the oscillatory flow that is also concerned in this work. The main components of the steady flow experimental apparatus, as shown in Fig. 6, are a heat exchanger, a hot water flow loop, an air compressor, measurement devices and a data acquisition system. The purpose of the hot water flow loop is to transport heat from a hot water bath to the heat exchanger by using hot water as a carrier. Control of the water flow rate can be achieved by either turning a valve attached to the loop just before the inlet of the heat exchanger (cf. valve V1 in Fig. 6) or by adjusting the height of the water container hung above the heat exchanger. The temperature at the inlet of the heat exchanger (T1) was controlled via the PID temperature controller that was also used for the oscillatory flow experiment. Each thermocouple probe T1 (water inlet) and T2 (water outlet) was inserted through a Swagelok T fitting and was fully immersed along the water stream. A water pump (Wilo-Smart 25/6) was used to circulate hot water flowing in the loop.

Air was used as a working medium flowing in a 2” stainless steel pipe through a given heat exchanger. In each test, the heat exchanger was held in the stainless steel housing connected to the stainless steel pipe. Sections ‘a’ and ‘b’ (see the test section detail in Fig. 6) are the vertical planes located in front of and behind the heat exchanger. There were three thermocouple probes installed in each plane. All thermocouple probes used in this experiment were of Type K stainless steel sheath with 1.0 mm diameter and 150 mm in length. A compressed air source supplies air through the 2” stainless steel pipe. Air flow velocity was obtained from an ISO round nose Pitot-static tube, which was installed at about 1.5 m downstream, away from the heat exchanger to avoid flow disturbance (BS1042, 1973; Robinson et al., 2004). The pressure value from the Pitot-static tube was read by a micro manometer (DP measurement, model TT370s) and converted into air flow rate. One thermocouple probe was also mounted behind the Pitot-static tube to estimate air properties from the measured temperature for the air mass flow rate calculation.

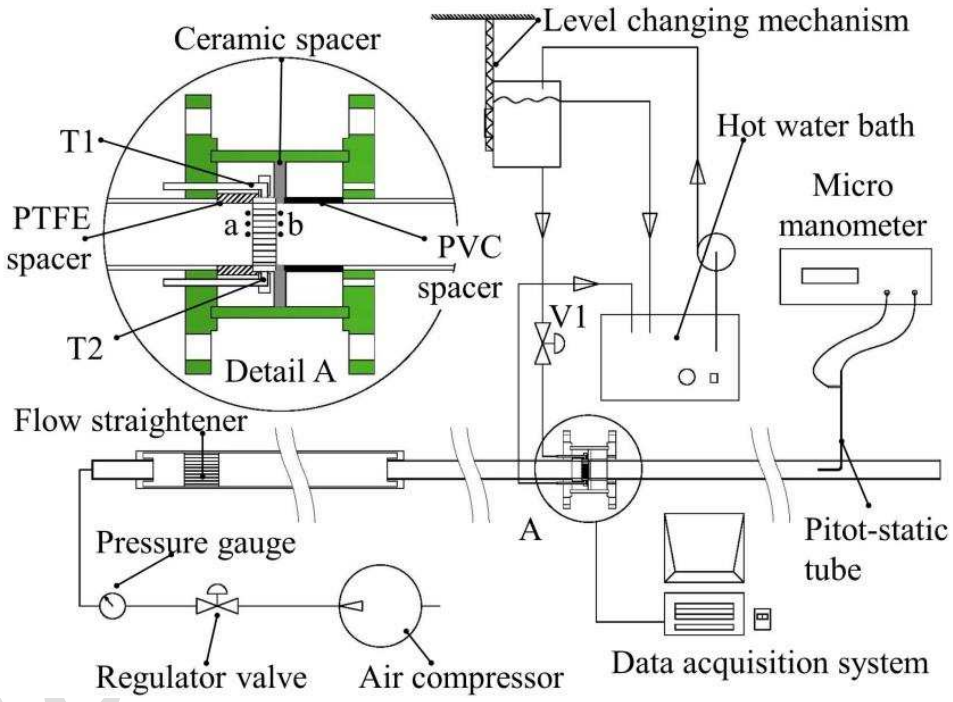

Fig. 6: Schematic diagram of the experimental apparatus for the steady flow arrangement.

3. Experimental procedure

The heat transfer performance in oscillatory flow is influenced by parameters such as displacement amplitude (ξ_a), fin length (L), fin spacing (D) and thermal penetration depth (δ_κ). The gas displacement amplitude (ξ_a) is the ideal distance when the gas particles move in an empty resonator. Inside the heat exchanger, the gas moves at a higher displacement amplitude, ξ_a/σ due to the

porosity (σ) of the heat exchanger or the reduced flow area. A small gap (2g = 5 mm) was left between the hot and cold heat exchangers to prevent the thermal contact. Thus, from the heat transfer point of view, the effective gas displacement inside a heat exchanger is (ξ_a - g)/σ. In the normalized term, there are two parameters for the geometry of the heat exchangers, which are D/δ_k and $(\xi_a - g)/(\sigma L)$. To investigate the effects of D/δ_k and $(\xi_a - g)/(\sigma L)$ on the heat transfer performance, measurements for the heat transfer rate were carried out, when these two dimensionless parameters varied.

3.1 Oscillatory flow experiment

The experiment was conducted with a combination of two selected heat exchangers which were installed in the heat exchanger housing. After installing the selected heat exchangers in the test section and assembling the heat exchanger housing with the resonator, some air would still remain in the system. As the working fluid in this study was pure helium gas, the remaining air in the resonator was removed by a vacuum pump.

One of the variables to be controlled in the experiment was the normalized fin spacing which is the ratio of fin spacing (D) to the thermal penetration depth (δ_k). The latter is defined by Eq.(1) and it clearly depends on both the pressure (through changes in density) and the frequency.

$$\delta_k = \sqrt{\frac{2k}{\omega \rho_m c_p}} \tag{1}$$

where k, ρ_m, c_p and ω are the thermal conductivity, density and isobaric specific heat of helium gas and the angular frequency. The quantity δ_k is the perpendicular distance from the plate surface, within which heat can diffuse through the gas during a time which is of the order of an oscillation period, $T = 1/f$, where f is the oscillation frequency.

According to Swift (2001), the optimal value of the fin spacing is about two to four times the thermal penetration depth $(2 \le D/\delta_k \le 4)$. Hence, the value of normalized fin spacing (D/δ_k) in this study ranged from 1.0 to 6.0 – which covered the suggested value. However, the highest D/δ_k for set 'A' heat exchanger was 3.5 as it was limited by the maximum design mean pressure of the experimental apparatus.

Another key parameter that influences heat transfer is gas displacement amplitude (ξ_a) which is defined by:

$$\xi_a = \frac{u_1}{\omega} = \frac{P_a \sin(k_w x)}{\omega \rho_m a} \quad (2)$$

where u_1 is the velocity amplitude and ω is the angular frequency of the oscillation. P_a is the pressure amplitude measured at the pressure anti-node of the wave, $k_w (= 2\pi/\lambda)$ is the wave number with λ being the wave length, ρ_m is the mean density, x is the distance from the pressure anti-node to the location of heat exchanger, and a is the sound speed in a working fluid.

Swift (1988) proposed that heat exchangers should have a length of peak-to-peak displacement amplitude $(L = 2\xi_a)$. In this experiment, the ratio of $(\xi_a - g)/(\sigma L)$ started from about -0.03. The negative value represents the peak-to-peak displacement that is shorter than the gap (2g). The upper bound of $(\xi_a - g)/(\sigma L)$ was selected to achieve 1.5. This selection aimed to cover the value $(\xi_a - g)/(\sigma L) = 0.5$ which was suggested by Swift (1988). In some conditions, however, the experiment could not be carried out on a high $(\xi_a - g)/(\sigma L)$ ratio due to the limitations of the driver excursion.

At the system mean pressure corresponding to a given D/δ_k, the driver was set to operate at the resonance frequency. The desired $(\xi_a - g)/(\sigma L)$ can be achieved by adjusting the driver piston displacement amplitude through the driver controller to increase or decrease the gas displacement amplitude. To proceed with the experiment, heat was delivered into the hot heat exchanger using hot water as a carrier. At a selected temperature, for instance 40^{o}C, the water temperature was monitored at the inlet of the hot heat exchanger. The temperature at this location was also the input signal for the PID temperature controller. In the cold heat exchanger, water at 22^{o}C was used to absorb and carry heat away from the system. The mass flow rate of hot and cold water were, respectively, maintained at 1.5 and 2.5 g·s^{-1} which was obtained by weighing the mass of collected water over time. Data collected in the current measurement included the temperature from all thermocouple probes according to Fig. 4, hot and cold water mass flow rate and acoustic pressure. Data acquisition was initiated in order to acquire temperature data when the system was in steady state condition. The data sampling rate of the acquisition system was set at 10 Hz in order to collect 2,000 data points over 3 minutes and 20 seconds. The procedure described previously applies to one

data point in a single operating condition. At the same operating condition, the measurement was repeated two more times. Data to be used for subsequent analysis were obtained from the average value of the three repeated measurements.

The next test point was completed by exciting the driver to achieve a higher gas displacement amplitude corresponding to the required $(\xi_a - g)/(\sigma L)$. The measurement for a selected value of D/δ_k is completed when the data collection is carried out for the whole range of $(\xi_a - g)/(\sigma L)$ considered. Once the measurement is completed a given D/δ_k, the next cycle is carried out at a next value of D/δ_k. A desired value of D/δ_k can be achieved by pressurizing the system with helium gas corresponding to the desired δ_k. After all experimental data for the inlet temperature of 40^oC was obtained, the subsequent measurements were performed for the hot heat exchanger inlet temperatures of 60 and 80^oC. This experiment was designed to be performed on three configurations of heat exchanger. To complete the test on the other two configurations, the first set of heat exchanger was removed and replaced by the new set. After installing the new configuration and assembling the test section, the leakage test and the removal of air from the resonator were carried out. The experimental procedure for the rest of the heat exchangers was similar to that explained above.

3.2 Steady flow experiment

In order to determine heat transfer performance in an oscillatory flow condition, the value of the water side heat transfer coefficient (h_i) needs to be known in advance. The experiment in steady flow conditions was introduced as follows. To carry out one batch of steady flow tests, a selected heat exchanger was installed in the stainless steel housing. Heat was supplied to the heat exchanger by hot water flowing inside the tube while the air flowing through fins absorbed and carried heat away from the test section. According to Fig. 6, air temperatures at upstream and downstream of the heat exchanger were obtained from thermocouples at sections ‘a’ and ‘b’, while thermocouples T1 and T2 were also used to measure the inlet and outlet temperature of the water, respectively. Water mass flow rate through the heat exchanger was obtained by weighing the mass of collected water and dividing it by the time period elapsed.

The first test on the heat exchanger with a fin spacing of 0.7 mm was performed at the lowest water inlet temperature of 40^oC. The water pump was turned on to circulate hot water through the heat exchanger loop. While waiting for the temperature to reach the set value, the water mass flow rate

was adjusted either by controlling a valve (cf. valve V1 in Fig. 6) or by changing the level of the water storage container that hung above the heat exchanger.

As far as the air side is concerned, the air compressor was turned on and left running until it reached its maximum pressure capacity. The air flow rate was set to start the test at the minimum flow rate. Air flow rate was controlled by using a regulator valve on the air compressor. After running the system for a period of time, the operator should monitor temperature variation for all measuring points. If the temperature profile exhibits stable trend, the flow rates of water and air are checked to make sure they are flowing at the required values. When the temperature and flow rate are achieved, the temperature data collection begins by initiating the data acquisition system. This procedure constitutes the measurement of one data point. The next test was carried out by slightly increasing the water flow rate. The range of the water mass flow rate must cover the flow rate designed for the oscillatory flow experiment. The next sets of measurement were performed at a higher air flow rate and the cycle was repeated. When the test at the maximum air flow rate and a water inlet temperature at 40^{o}C was completed, the experiment was then carried out for the higher temperatures of 60 and 80^{o}C. The whole procedure was repeated for heat exchangers with fin spacing of 1.4 and 2.1 mm to complete the data collection in the steady flow experiment.

4. Data reduction

Data reduction for steady flow experiment is presented first in order to obtain the water side heat transfer coefficient (h_i). It will facilitate the heat transfer performance evaluation in oscillatory flow which is illustrated in Section 4.2.

4.1 Steady flow

The aim of the current study is to develop measurement techniques for heat transfer when the working gas experiences an oscillating flow. The heat transfer coefficient for water side (h_i) is required prior to calculating the heat transfer performance in oscillatory flow conditions. The data processing procedure to obtain h_i is described as follows. The heat transfer rate between hot water and air is calculated by:

$$\dot{Q}_w = \dot{m}_w c_{p,w} (T_{w,i} - T_{w,o}) \quad (3)$$

or

$$\dot{Q}_a = \dot{m}_a c_{p,a} (T_{a,o} - T_{a,i}) \quad (4)$$

The subscripts w, a, i and o in above equations denote water, air, and the location at the inlet and outlet of the fluid stream, respectively. $c_{p,w}$ and $c_{p,a}$ are specific heat capacity at constant pressure of water and air. The mass flow rate of water is achieved by weighing the mass of collected water and dividing it by the elapsed time. On the air side, mass flow rate is obtained from:

$$\dot{m}_a = \rho_a A V_{avg} \tag{5}$$

where ρ_a, A and V_{avg} are air density, air flow area and average air flow velocity. The air flow velocity over the Pitot-static tube in this experiment was limited to subsonic velocity and the point velocity at the Pitot-static tube was estimated from the equation (Klopfenstein, 1998):

$$V = \sqrt{2\Delta P / \rho_a} \tag{6}$$

where ΔP denotes the difference of total pressure and static pressure which is obtained from the micro manometer readings. As the sensing tip of the Pitot tube is located at the centre of the tube, the air flow velocity estimated from Eq.(6) constitutes the maximum flow velocity (V_{max}). It will be necessary to estimate the average velocity from the maximum velocity in order to calculate air mass flow rate. The average velocity is simply obtained from $V_{avg} = V_{max}/2$ for Reynolds number below 2,300 (Çengel and Cimbala, 2006).

According to the current experimental data, the Reynolds number of air based on the pipe diameter is greater than 2,300. Thus, the flow of air in the pipe falls in a turbulent flow region. The equation to estimate the average flow velocity for turbulent flow is given as (Rennels and Hudson, 2012):

$$V_{avg} = V_{max} / (1 + 1.3258\sqrt{f_s}) \tag{7}$$

The friction factor (f_s) appearing in Eq.(7) can be calculated from the equation given by S. E. Haaland in 1983 as (Çengel and Cimbala, 2006):

$$\frac{1}{\sqrt{f_s}} = -1.8 \log\left[\frac{6.9}{Re} + \left(\frac{\varepsilon_s / D}{3.7}\right)^{1.11}\right] \tag{8}$$

where the absolute roughness (ε_s) of the PVC pipe is 0.0015 mm (Rennels and Hudson, 2012). To obtain the average air flow velocity, an iterative process in Eq.(7) and (8) is required as the unknown air flow velocity is integrated in the Reynolds number in Eq.(8).

The heat transfer in the heat exchanger used in the current experiment involves the thermal resistance consisting of three parts: the resistance for heat transfer from water to the wall of copper tube, thermal resistance of copper tube and the resistance for heat transfer from copper tube to air. It is useful to apply an overall heat transfer coefficient concept as (Paek et al., 2005 and Mao et al., 2011):

$$\frac{\dot{Q}}{LMTD_{STD}} = UA = \frac{1}{R} = \frac{1}{\frac{1}{\eta_o (aRe_{o,STD}^{b}) A_o} + R_{tube} + \frac{1}{(cRe_i^{d}) A_{t,i}}} \tag{9}$$

In Eq.(9), air side Reynolds number ($Re_{o,STD}$) is based on the fin spacing hydraulic diameter (D_h), while water side Reynolds number (Re_i) is based on copper tube inside diameter (D_i). The logarithmic mean temperature difference ($LMTD_{STD}$) is given by:

$$LMTD_{STD} = F \frac{(T_{w,i} - T_{a,o}) - (T_{w,o} - T_{a,i})}{\ln\left(\frac{T_{w,i} - T_{a,o}}{T_{w,o} - T_{a,i}}\right)} \tag{10}$$

The correction factor (F) is introduced so that the $LMTD_{STD}$ is suitable for the cross flow arrangement. It is approximately 0.98 (Çengel, 1997). Thermal resistance of copper tube is obtained by:

$$R_{tube} = \ln(r_2 / r_1) / 2\pi L_T k \tag{11}$$

where r_2 and r_1 are the outside and inside tube radii. L_T denotes the effective tube length where the heat transfer to/from the air occurs and k is the thermal conductivity of the copper tube.
The overall fin efficiency (η_o) is obtained from (Incropera, 2006):

$$\eta_o = 1 - \frac{A_f}{A_o}(1 - \eta_f) \tag{12}$$

where A_f and A_o are fin surface area and air side heat transfer area (fin surface area plus the area of copper tube contacts with air). The efficiency of a single fin (η_f) is calculated from:

$$\eta_f = \frac{\tanh(mL_c)}{mL_c} \tag{13}$$

where mL_c is expressed by:

$$mL_c = \sqrt{\frac{h_0 \cdot \Pi}{k \cdot A_{fc}}} \cdot L_c \tag{14}$$

In Eq.(14), h_o is the convective heat transfer coefficient and k is the thermal conductivity of fin material. Geometrical parameters A_{fc}, Π and L_c denote fin cross sectional area, fin cross sectional perimeter and corrected fin length, respectively. When the fin is considered having convection heat transfer at its tip, the corrected fin length (L_c) can be found from:

$$L_c = L + (t/2) \tag{15}$$

where L and t are the fin length and fin thickness, respectively.

From Eq.(9), $\dot{Q}$ and $LMTD_{STD}$ are calculated from Eq.(3) and Eq.(10) using measured data. Then, parameters a, b, c and d are obtained by non-linear surface fitting using the simplex method in software package 'Origin'. The heat transfer coefficient of the air side ($h_{o,STD}$) and the water side (h_i) can be defined as:

$$h_{o,STD} = aRe_{o,STD}^{b} \tag{16}$$

$$h_i = cRe_i^{d} \tag{17}$$

4.2 Oscillatory flow

In oscillatory flow experiment, heat carried by the hot water stream inside the tube of the hot heat exchanger is transferred to the oscillating gas. The oscillating gas works as a carrier to transport heat between the hot and cold heat exchangers. Then, the heat is absorbed at the cold heat

exchanger and ejected to the external heat sink. Heat transfer rate in oscillatory flow is calculated from the water side of hot heat exchanger following Eq.(3). The measurement on cold heat exchanger is possible but less accurate. This is due to the cold water flow rate being maintained at a higher value than that of the hot water. As a result, the temperature difference between the inlet and exit of the cold heat exchanger was small, leading to high uncertainty in the heat transfer rate.

Considering the heat leakage, heat conduction from the heat exchangers through the helium gas, insulator and resonator pipe to the surrounding environment may exist. This can be calculated from the Fourier equation using temperature at points T_a, T14 and T16 (see Fig. 4). The relationship between the leakage heat and the heat transfer rate measured at the water side of the hot heat exchanger is plotted in Fig. 7 and the correlation is shown in Eq.(18). The correlation was obtained using Nelder-Mead downhill simplex method for the non-linear curve fitting for its stability (Seber and Wild, 2003). From the fitting, a coefficient of determination R^2 is 0.86.

$$\dot{Q}_{leak} / \dot{Q}_{hot} \times 100 = 27.6 \times \dot{Q}_{hot}^{-0.85} \tag{18}$$

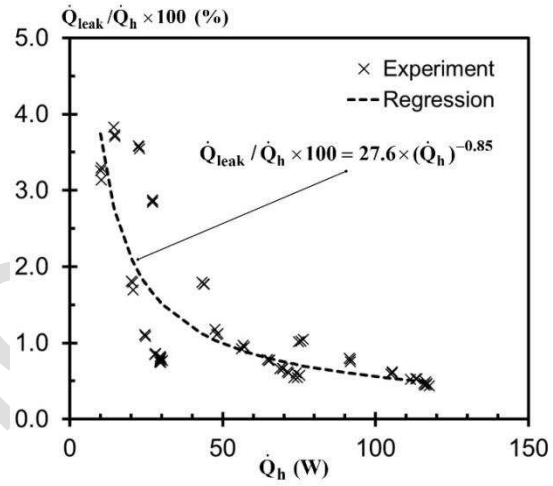

Fig. 7: The percentage of leakage heat $((\dot{Q}_{leak} / \dot{Q}_{hot}) \text{x} 100(\%))$ as a function of heat transfer rate measured at the hot heat exchanger $(\dot{Q}_{hot})$.

Then the heat transfer rate measured on the hot heat exchanger was subtracted by the heat leakage before the subsequent analysis. From the obtained heat transfer rate, dimensionless heat transfer coefficient in terms of Colburn-j factor for the gas side can be evaluated by:

$$j = \frac{Nu}{Re_1 Pr^{1/3}} = \frac{h_{o,OSC}(D_h / k)}{Re_1 Pr^{1/3}} \tag{19}$$

Acoustic Reynolds number (Re_1) is expressed by:

$$Re_1 = \frac{\rho D_h u_1}{\mu} \tag{20}$$

where u_1 denotes acoustic velocity amplitude.

To find the gas side heat transfer coefficient in oscillatory flow ($h_{o,OSC}$), the overall heat transfer coefficient is employed on the hot heat exchanger as follows:

$$\frac{\dot{Q}}{LMTD_{OSC}} = UA = \frac{1}{\frac{1}{\eta_o h_{o,OSC} A_o} + R_{tube} + \frac{1}{h_i A_i}} \tag{21}$$

The log-mean temperature difference $LMTD_{OSC}$ is defined as:

$$LMTD_{OSC} = \frac{\left(T_{w,o} - T_{w,i}\right)}{\ln\left(\frac{T_b - T_{w,i}}{T_b - T_{w,o}}\right)} \tag{22}$$

T_b is the temperature of the gas at section 'b' according to Fig. 4, while $T_{w,i}$ and $T_{w,o}$ denote the temperature of water measured at the inlet (T10) and exit (T11) of the hot heat exchanger, respectively. The heat transfer coefficient for the water side (h_i) can be obtained from Eq.(17) which was developed from the steady flow experiment.

5. Measurement uncertainty

Measurement uncertainty is performed to estimate errors in the experimental results. The uncertainty consists of several components which can be categorized into two groups: precision or random uncertainty, and systematic or fixed uncertainty (Rood and Telionis, 1991 and Kim et al., 1993). From Eq.(3), the uncertainty $(U_{\dot{Q}})$ of heat transfer rate $(\dot{Q})$ is given by the combination of a precision uncertainty $(s_{\dot{Q}})$, and a systematic uncertainty $(b_{\dot{Q}})$.

$$U_{\dot{Q}} = (s_{\dot{Q}}^2 + b_{\dot{Q}}^2)^{1/2} \tag{23}$$

The estimations of the precision and systematic uncertainty are made according to the error propagation equation (Kline and McClintock, 1953) as follows.

$$s_{\dot{Q}}^2 = (\partial\dot{Q}/\partial\dot{m})^2 s_{\dot{m}}^2 + (\partial\dot{Q}/\partial c_p)^2 s_{c_p}^2 + (\partial\dot{Q}/\partial T_o)^2 s_{T_o}^2 + (\partial\dot{Q}/\partial T_i)^2 s_{T_i}^2 \tag{24}$$

and

$$b_{\dot{Q}}^2 = (\partial\dot{Q}/\partial\dot{m})^2 b_{\dot{m}}^2 + (\partial\dot{Q}/\partial c_p)^2 b_{c_p}^2 + (\partial\dot{Q}/\partial T_o)^2 b_{T_o}^2 + (\partial\dot{Q}/\partial T_i)^2 b_{T_i}^2 \tag{25}$$

where $s_{\dot{m}}$, s_{To} and s_{Ti} are the elemental precision uncertainty of $\dot{m}$, T_o and T_i, respectively. The partial derivations appeared in Eq.(24) and (25) are the sensitivity coefficient which represent the change of the result $(\dot{Q})$ when the value of a particular elemental measurement parameter is varied. The uncertainties of elemental parameters are described as follows.

5.1 Uncertainty of water mass flow rate measurement

The water mass flow rate $(\dot{m})$ present in Eq. (3) is obtained from the mass of collected water (m) over the elapsed time (t) by $\dot{m} = m/t$. Applying the error propagation approach, the precision uncertainty $(s_{\dot{m}})$ and systematic uncertainty $(b_{\dot{m}})$ of the water mass flow rate measurement can be found by:

$$s_{\dot{m}}^2 = \left(\frac{\partial\dot{m}}{\partial m}\right)^2 s_m^2 + \left(\frac{\partial\dot{m}}{\partial t}\right)^2 s_t^2 \tag{26}$$

and

$$b_{\dot{m}}^2 = \left(\frac{\partial\dot{m}}{\partial m}\right)^2 b_m^2 + \left(\frac{\partial\dot{m}}{\partial t}\right)^2 b_t^2 \tag{27}$$

where s_m and s_t are the precision uncertainty of mass and time measurement, and b_m and b_t are the systematic uncertainty of mass and time measurement, respectively.

In mass flow rate measurement, the systematic uncertainty of mass (b_m) and time (b_t) measurements are omitted because the digital scale and the stop watch were calibrated. Precision uncertainty for mass (s_m) and time (s_t) measurement is calculated from a series of repeated observations using statistical methods. The precision uncertainty of mass measurement (s_m), due to repeatability, is

evaluated through the sample standard deviation (S_m) of the repeated mass measurement results from Eq. (28) (Miller, 2002).

$$s_m = S_m / \sqrt{N} \tag{28}$$

where N is a number of samples. For the measurement of elapsed time, the precision uncertainty (s_t) arises from the reaction time of the operator when pressing the start/stop button of the stop watch. The procedure to evaluate for s_t follows the instruction as reported by Gust et al. (2004).

5.2 Uncertainty of isobaric specific heat of water

In this experiment, the variable isobaric specific heat capacity (c_p) was estimated by an equation (Richardson, 2010). The specific heat value of water was calculated using the average temperature of the inlet and exit of a heat exchanger as an input value. Thus, there may be an uncertainty in the specific heat capacity estimated from the average temperature. As the value of c_p is obtained from the equation, the precision uncertainty (s_{cp}) is neglected. Another source of error stems from the accuracy of the curve-fitting equation. This kind of error is considered to be a systematic uncertainty in the specific heat capacity value. In some published sources (Angell et al., 1982; Archer and Carter, 2000), the uncertainty of specific heat capacity is presented in the form of a percentage departure of experimental data from the values calculated from the curve-fitting equation. According to Wagner (2002), the systematic uncertainty of water specific heat capacity (b_{cp}), estimated at 95% confidence, corresponding to the current experimental conditions is ±0.4% of the calculated value.

5.3 Uncertainty of temperature measurement

In order to calculate the heat transfer rate according to Eq. (3), the measurement of water temperature at the inlet and exit points needs to be acquired. Similar to other variables, the errors inherent in temperature measurement originate from the precision and systematic errors. The precision uncertainty is estimated from the standard deviation of samples for temperature measurement. Systematic uncertainty is embedded in temperature measurements. The value of systematic uncertainty does not vary and it cannot be directly determined by measurements or any statistical technique. The systematic uncertainty is influenced by the calibration standard of the thermocouple probes which is achieved from the thermocouple specification supplied by the

manufacturer. Following the procedure suggested by Kim et al. (1993) and Coleman and Steele (2009), the systematic uncertainty for temperature measurement (b_{Ti} and b_{To}) obtained from type K thermocouple probes used in this experiment is evaluated at $\pm 0.55^{o}$C based on the 95% confidence level.

5.4 Uncertainty of heat transfer rate

From the elemental uncertainty described in section 5.1 through to 5.3 and shown in Table 3, the uncertainty of heat transfer rate is obtained using Eq. (23). The overall uncertainty of the experimental heat transfer rate results evaluated at 95% confidence level has a range of 4.5-20.1%. The uncertainty is higher for a low heat transfer rate when the temperature difference between the inlet and outlet of water stream is as low as 1.0^{o} C. Measurement uncertainty is evaluated for all heat exchangers at all operating conditions. Error bars are included in the heat transfer rate results of all set of heat exchangers (see Fig. 10 and Fig. 11). As previously stated in Section 4.2, the measured heat transfer rate was subtracted by the heat leakage estimated from Eq. (18) and Fig. 7 before further analysis. The heat leakage evaluation is another source of uncertainty. Nevertheless, the heat leakage is considerably small compared to the heat transfer rate under investigation, approximately 1.0% for heat transfer rates above 50 W, which is attributed to good insulation. The uncertainty in the heat leakage is obtained from the standard deviation of the correlation.

Table 3: Parameter uncertainties estimated at 95% confidence.

Parameters	Precision uncertainty	Systematic uncertainty
Mass of water	±0.3 g	-
Elapsed time	±0.2 s	-
Specific heat capacity	-	±0.4%
Inlet temperature	$\pm 0.030^{o}$C	$\pm 0.55^{o}$C
Outlet temperature	$\pm 0.032^{o}$C	$\pm 0.55^{o}$C
Heat leakage	-	±0.35W
Combined uncertainty	4.5 - 20.1%	

6. Results and discussion

In steady flow experiment, water side (h_i) and gas side ($h_{o,STD}$) heat transfer coefficient are obtained from data regression. They are presented as a function of Reynolds number. It is followed by the heat transfer analysis in oscillatory flow conditions, where the dependences of temperature

measured at different locations, heat transfer rate and Coburn-j factor on $(\xi_a - g)/(\sigma L)$ and D/δ_k are presented.

6.1 Heat transfer in steady flow

The heat transfer coefficient of the air side ($h_{o,STD}$) and the water side (h_i) can be found from Eq.(16) and (17), respectively. The coefficients a, b, c and d for each heat exchanger are obtained by non-linear surface fitting from Eq.(9) using the simplex method in software package 'Origin' and are presented in Table 4. Figure 8(a) shows the variation of the water side heat transfer coefficient (h_i) for all heat exchangers with a water side Reynolds number (Re_i). In Fig. 8(b), the air side heat transfer coefficients ($h_{o,STD}$) of all heat exchangers are plotted against the steady flow Reynolds number of air ($Re_{o,STD}$), which is based on the hydraulic diameter (D_h) of fin spacing.

Table 4: Regression results for the steady flow experiment.

Parameters	Heat exchanger		
	HEX-1	HEX-2	HEX-3
Water side			
h_i	$h_i = 69.13Re_i^{0.44}$	$h_i = 43.87Re_i^{0.50}$	$h_i = 38.00Re_i^{0.51}$
Re_i	$314 < Re_i < 2534$	$319 < Re_i < 3086$	$307 < Re_i < 4247$
Air side			
$h_{o,STD}$	$h_{o,STD} = 3.68Re_{o,STD}^{0.69}$	$h_{o,STD} = 3.21Re_{o,STD}^{0.68}$	$h_{o,STD} = 18.04Re_{o,STD}^{0.32}$
$Re_{o,STD}$	$67 < Re_{o,STD} < 879$	$109 < Re_{o,STD} < 1172$	$154 < Re_{o,STD} < 732$
Data points	200	175	162
Regression R^2	0.92	0.96	0.90

6.2 Heat transfer in oscillatory flow

In oscillatory flow conditions, temperature measurement of relevant locations is presented. The influences of $(\xi_a - g)/(\sigma L)$ and D/δ_k on heat transfer rate $(\dot{Q})$ are discussed. The dimensionless heat transfer coefficient, Colburn-j factor, is also presented as a function of acoustic Reynolds number (Re_1).

6.2.1 Temperature information

Temperature profiles at locations of interest are presented in order to observe the heat transfer process as a function of $(\xi_a - g)/(\sigma L)$ and to determine the heat leakage from the heat exchanger to

the environment. Fig. 9(a) and (b) show the variation of temperatures measured from different locations at the test section plotted against $(\xi_a - g)/(\sigma L)$ for set 'A' heat exchanger (0.7 mm HEX) with hot water inlet temperature ($T_{h,i}$) of 80 ^{o}C when D/δ_k is 1.5 and 3.5, respectively. The first data point from the left of each curve was collected at stationary gas conditions (no excitation from the driver). Temperature measurement points can be found referring to Fig. 4. In Fig. 9(a) and (b), the top and bottom lines are the inlet temperature of hot ($T_{h,i}$) and cold ($T_{c,i}$) heat exchangers, respectively. Both lines are virtually stable as they are maintained at given temperatures. When the gas parcels start oscillating, the transported heat between the hot and cold side heat exchangers is noticed. This is observed from the span of temperature difference between the inlet and exit of each heat exchanger which becomes larger. The increase of these temperature spans, however, is less pronounced when $(\xi_a - g)/(\sigma L)$ is higher than 0.5.

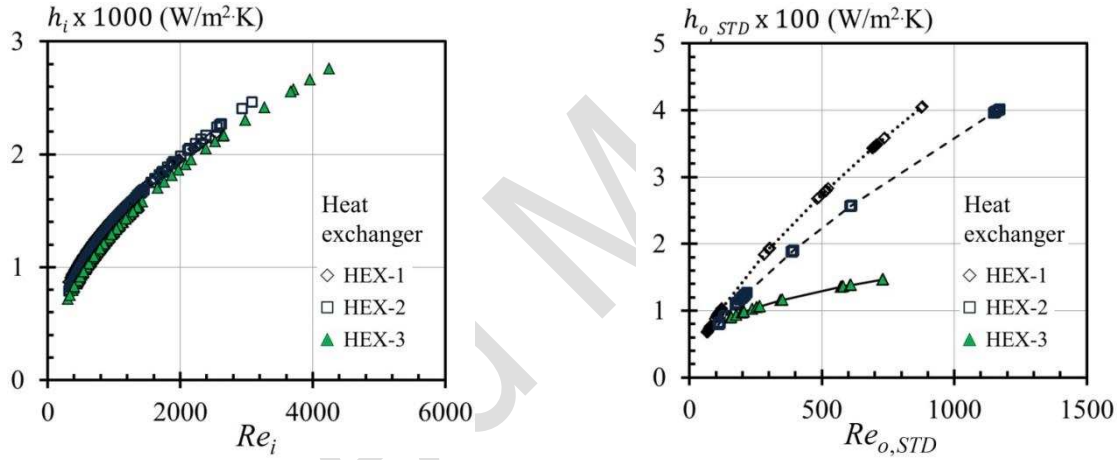

(a) (b)

Fig. 8: Heat transfer coefficient of the water side (h_i) (a) and of the air side ($h_{o,STD}$) (b).

Generally, the gas temperature at plane 'a' (T_a) measured at the front of the hot heat exchanger gradually decreases as $(\xi_a - g)/(\sigma L)$ increases. This is because the cold gas from the cold heat exchanger penetrates the hot heat exchanger absorbing and carrying heat on its returning cycle. Simultaneously, the gas at plane 'c' (T_c), located just behind the cold heat exchanger, is warmer at a higher $(\xi_a - g)/(\sigma L)$ because the cold heat exchanger receives more heat from the hot heat exchanger. The temperature profiles of oscillating gas T_a, T_b and T_c are closer to each other and almost stable when $(\xi_a - g)/(\sigma L) > 1.0$. This may indicate that the heat transfer between two heat exchangers is reaching its maximum performance and $(\xi_a - g)/(\sigma L)$ is likely to be less influential on the heat transfer. This is consistent with the outlet temperature of both hot and cold water streams,

where the slopes are lower for $(\xi_a - g)/(\sigma L)$ higher than 0.5 and likely to level off beyond $(\xi_a - g)/(\sigma L) > 1.0$.

It can be noted that the temperature profiles for T_a, T_b and T_c at higher D/δ_k are closer to each other than those at the lower D/δ_k. For example, with $(\xi_a - g)/(\sigma L)$ at about 1.5, the curves of T_a, T_b and T_c for $D/\delta_k = 3.5$ in Fig. 9(b) are closer to each other than that for $D/\delta_k = 1.5$ in Fig. 9(a). This may imply that a higher D/δ_k provides a higher heat transfer performance. The results for heat exchanger sets 'B' (1.4 mm HEX) and 'C' (1.4 mm HEX) (not shown here) also exhibit the similar trend with that shown in Fig. 9.

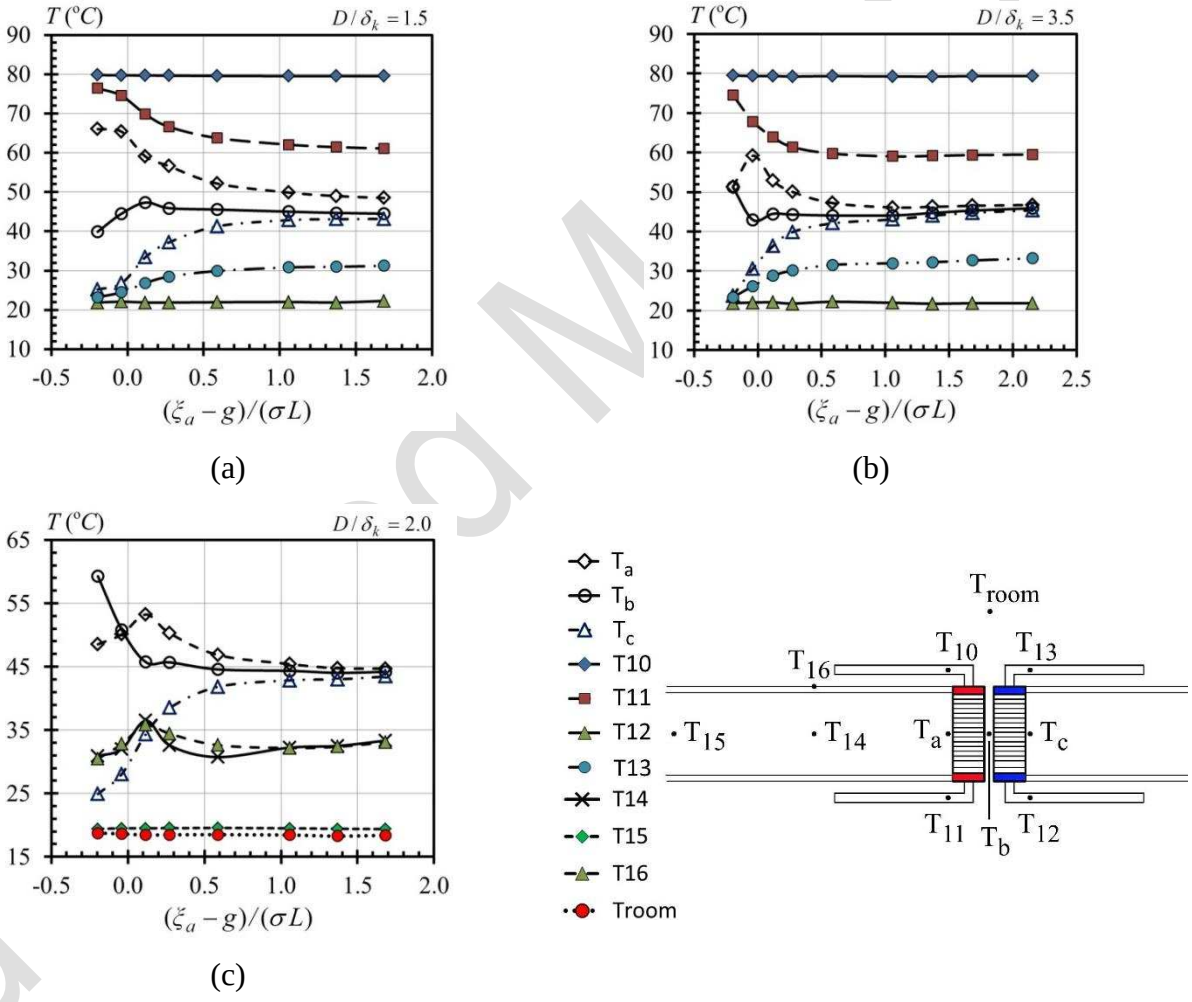

Fig. 9: Variation of temperature measured at different locations versus $(\xi_a - g)/(\sigma L)$ for set 'A' heat exchanger.

Considering the heat leakage prevention, insulation was provided as much as possible. However, heat leakage from heat exchanger to the environment may exist during the experiment and it needs to be determined. As shown in Fig. 4, thermocouple probes T14 and T15 were installed in front of

the hot heat exchanger in order to estimate the conductive heat transfer through the gas. The temperature of the external surface of the stainless steel resonator, detected by T16, and room temperature were also collected simultaneously.

Fig. 9(c) shows temperature variation on set 'A' heat exchanger for selected locations. It can be seen that the curves for temperature of gas measured at the point in front of the hot heat exchanger (T14) and of the resonator external surface (T16) have similar trend with the gas temperature measured at section 'a' (T_a) but smaller in magnitude. This indicates some heat leakage via the conduction from the hot heat exchanger through the gas and the stainless steel pipe. The temperature of gas further away from the hot heat exchanger was obtained from the thermocouple probe T15 and found to be very close to room temperature (T_{room}). Thus, the conductive heat transfer in gas from T14 to T15 was considered small. The relative heat leakage $(\dot{Q}_{leak})$ as a function of measured heat transfer rate $(\dot{Q}_{hot})$ was shown in Fig. 7. The heat transfer rate measured on the hot heat exchanger $(\dot{Q}_{hot})$ was then corrected by the heat leakage $(\dot{Q}_{leak})$ before subsequent analysis.

6.2.2 The influence of $(\xi_a - g)/(\sigma L)$ on heat transfer rate $(\dot{Q})$

The influence of $(\xi_a - g)/(\sigma L)$ on heat transfer rate $(\dot{Q})$ is investigated and shown in Fig. 10. The lines connecting the symbols are only for visual guidance. The heat transfer rate is evaluated on the hot side heat exchanger via Eq.(3). On every heat exchanger, the experiment was performed at various D/δ_k values ranging from 1.0 to 6.0 depending on the system capability.

In Fig. 10(a), the results for set 'A' heat exchanger (0.7 mm HEX) tested at 80°C hot water inlet temperature are shown. Heat transfer rate $(\dot{Q})$ is plotted versus the normalized gas displacement amplitude $(\xi_a - g)/(\sigma L)$ at various D/δ_k. Overall, for $(\xi_a - g)/(\sigma L) < 0.5$, the heat transfer rate increases rapidly with $(\xi_a - g)/(\sigma L)$. This is noted by the steep curves from the lowest $(\xi_a - g)/(\sigma L)$ to $(\xi_a - g)/(\sigma L) \approx 0.5$ for all D/δ_k. A plateau is usually reached for $(\xi_a - g)/(\sigma L) > 1.5$.

The significant growth of heat transfer rate for $(\xi_a - g)/(\sigma L) < 0.5$ is associated with the increase of the effective heat transfer area. For gas parcels that move a short distance where the peak-to-peak displacement amplitude is shorter than the spacing between two heat exchangers $((\xi_a - g)/(\sigma L) < 0)$, they only shuttle heat from one location to another within the same fin. The observed heat transfer

may be attributed to heat conduction through the gas. When the gas displacement amplitude increases, the proportion of gas parcels that have thermal contact with both heat exchangers within their oscillating cycle is larger, thus enhancing the heat transfer rate. The heat transfer increases steadily until $(\xi_a - g)/(\sigma L) \approx 0.5$ where all gas parcels that have thermal contact on one heat exchanger are able to reach the surface of the adjacent heat exchanger thus transferring heat between them. When $(\xi_a - g)/(\sigma L) > 0.5$, a fraction of gas particles jump from one heat exchanger and pass to the farthest edge of the next heat exchanger. Hence, such parcels do not contribute to the heat transfer between heat exchangers, and thus do not contribute to the heat transfer rate enhancement.

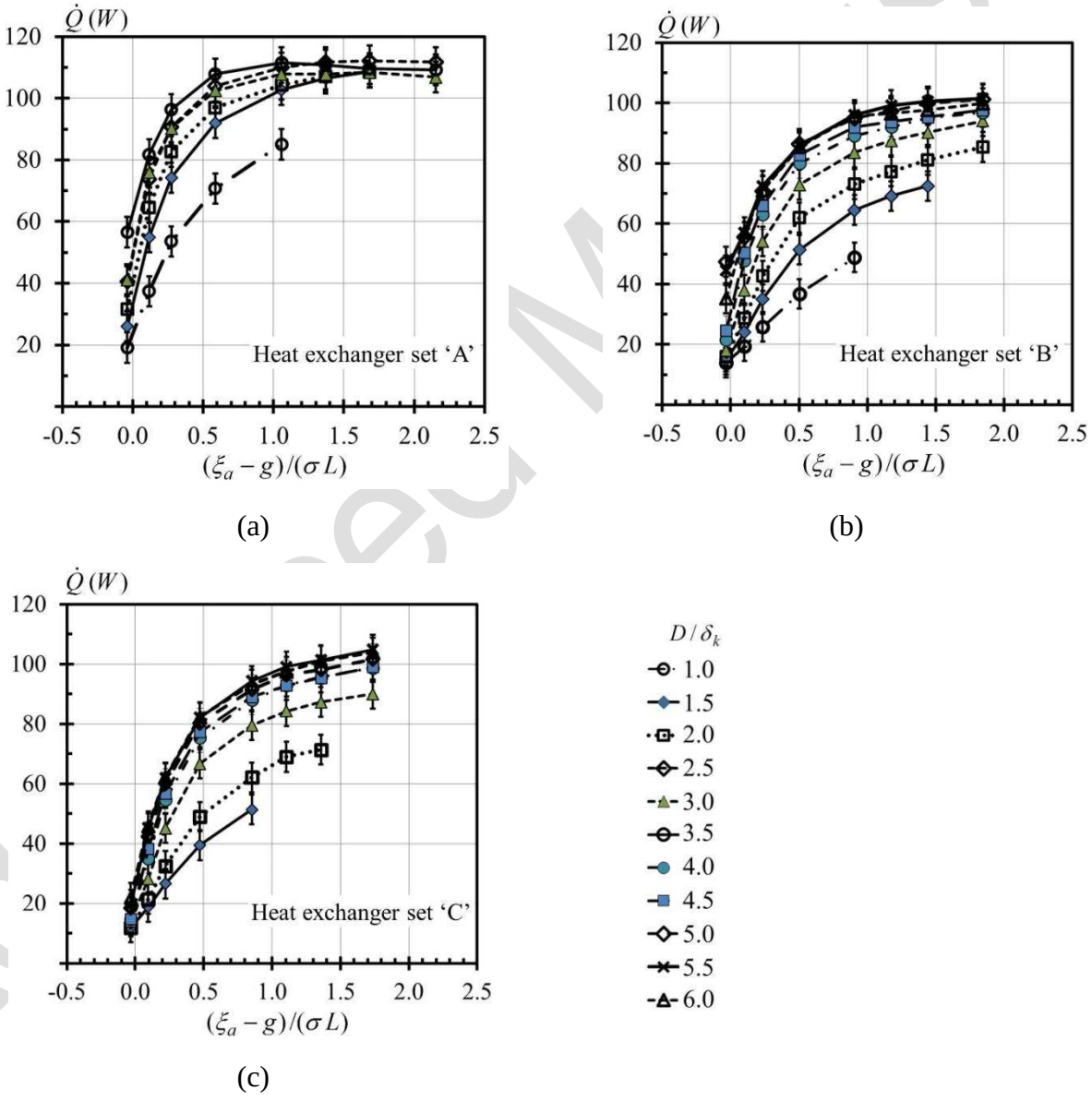

Fig. 10: Dependence of $\dot{Q}$ on $(\xi_a - g)/(\sigma L)$ at various D/δ_k for $T_{h,i} = 80^oC$.

It can be observed from Fig. 10(b) that the heat transfer rate on set 'B' heat exchanger (1.4 mm HEX) increases for $(\xi_a - g)/(\sigma L) < 0.5$, similar to what was observed for set 'A' heat exchanger but the rate of increase is smaller. The heat transfer rate continues to increase gradually for $(\xi_a - g)/(\sigma L) > 0.5$. In Fig. 10(c), the heat transfer rate on set 'C' heat exchanger (2.1 mm HEX) increases continuously with the increase of $(\xi_a - g)/(\sigma L)$ and tends to keep rising beyond $(\xi_a - g)/(\sigma L) > 1.5$. Theoretically, gas particles that oscillate with a $(\xi_a - g)/(\sigma L)$ higher than 0.5 should have no useful function in the heat transfer enhancement, as previously stated. The heat transfer observed beyond this point may be due to a longitudinal diffusive heat transfer from the gas to the heat exchangers. It is speculated that the gas in heat exchanger A may be fully heated to the temperature of the fins of the heat exchanger, so that the heat transfer rate become saturated, due to the less amount of gas allowed to pass through the heat exchanger, given the smaller fins spacing and a higher number of fins in heat exchanger. A more careful study of the heat transfer in the channel of similar geometry, preferably with temperature fields scrutinized, will be needed.

The experiments for the hot water inlet temperatures of 60 and 40^{o}C are also carried out. Their results are not shown here as they are similar to those observed at 80^{o}C, as described in relation to Fig. 10. In general, the heat transfer rate increases with the increase of $(\xi_a - g)/(\sigma L)$ for all sets of heat exchangers under test. This phenomenon is related to the increase in the effective heat transfer area when $(\xi_a - g)/(\sigma L)$ increases. Besides, gas parcels can shuttle heat over a distance of $(\xi_a - g)/\sigma$ in an oscillation cycle. For a fixed heat exchanger length L, the bigger $(\xi_a - g)/\sigma$, the greater the capacity of gas to transfer heat between heat exchangers.

6.2.3 The influence of D/δ_k on heat transfer rate $(\dot{Q})$

Data from the same measurements as those shown in Fig. 10 can be re-arranged to present the dependence of heat transfer rate $(\dot{Q})$ on D/δ_k. The relation of heat transfer rate $(\dot{Q})$ and D/δ_k for $T_{h,i}$ = 80^{o}C is presented for various values of $(\xi_a - g)/(\sigma L)$ as presented in Fig. 11. The lines connecting the symbols are only for visual guidance.

From the results for set 'A' heat exchangers (0.7 mm HEX) at $T_{h,i}$ = 80^{o}C shown in Fig. 11(a), it can be seen that $\dot{Q}$ steadily rises with D/δ_k for $1.0 < D/\delta_k < 2.5$ for all values of $(\xi_a - g)/(\sigma L)$. When $D/\delta_k > 2.5$, however, the values of $\dot{Q}$ decrease or remain unchanged for $(\xi_a - g)/(\sigma L) > 0.59$. The peak of $\dot{Q}$ for other $(\xi_a - g)/(\sigma L)$ may occur at $D/\delta_k > 5.0$, if the rig can withstand such a high mean

pressure, as were the case for the heat exchanger sets 'B' and 'C'. The influence of D/δ_k on $\dot{Q}$ for set 'B' heat exchanger (1.4 mm HEX) is shown in Fig. 11(b). The increase of $\dot{Q}$ with D/δ_k is observed for the value of D/δ_k up to 5.0. In general, it appears that $D/\delta_k = 5.0$ seems to be the peak of $\dot{Q}$ for most $(\xi_a - g)/(\sigma L)$ values. Fig. 11(c) shows the results for set 'C' heat exchangers (2.1 mm HEX). The overall trend is similar to that seen in set 'B' heat exchanger (1.4 mm HEX). However, the peak of $\dot{Q}$ for $(\xi_a - g)/(\sigma L) \geq 0.09$ tends to occur at $D/\delta_k = 5.5$, whereas the values of $\dot{Q}$ for $(\xi_a - g)/(\sigma L) = -0.03$ continue to increase with D/δ_κ. Generally speaking, the optimum $\dot{Q}$ for most conditions could be between $5.0 < D/\delta_\kappa < 5.5$. Compared to the recommended region of $2 \leq D/\delta_\kappa \leq 4$ (Swift, 2001), the optimal D/δ_κ obtained from the current study is slightly higher. This could be due to the physical construction of the heat exchangers used, in which tubes are connecting fins for heat supply and contribute a substantial amount to the overall heat transfer area, whereas in the literature, the optimal range of D/δ_κ is based on a numerical study of heat transfer between two parallel plates with a negligible thickness. The underlying mechanism of the difference is not clear.

6.2.4 Dimensionless heat transfer coefficient: Colburn-j factor

From the measured data for heat transfer in oscillatory flow, the gas side Colburn-j factor (j_{OSC}) was determined using Eq.(19). Fig. 12(a) shows the experimental results of Colburn-j factor as a function of acoustic Reynolds number (Re_1) for three sets of heat exchangers. In order to obtain the Colburn-j factor, the gas side heat transfer coefficient in oscillatory flow ($h_{o,OSC}$) is required which can be calculated from Eq. (21). The heat transfer effective area for the gas side (A_o) in Eq. (21) is the smaller value of the following, the area covered by the gas peak-to-peak displacement amplitude, and the gas side overall heat exchanger area. Generally speaking, the Colburn-j factor (j_{OSC}) decreases as the acoustic Reynolds number (Re_1) increases.

It can be identified from Fig. 12(a) that the data points are located in three clusters corresponding to the hot heat exchanger fin spacing. At the same acoustic Reynolds number (Re_1), the Colburn-j factor (j_{OSC}) values from set 'C' heat exchangers (2.1 mm HEX) are higher than those from set 'B' heat exchangers (1.4 mm HEX) and set 'A' heat exchangers (0.7 mm HEX), respectively. It should be noted that lines are only for visual guidance and the different symbols of the result for each heat exchangers represent the information obtained from different mean pressures, thus different thermal penetration depths (δ_k). It is observed that the results from different δ_k on one heat exchanger are

distributed along the aiding line which may indicate that thermal penetration depth does not have significant effect on the Colburn-j factor.

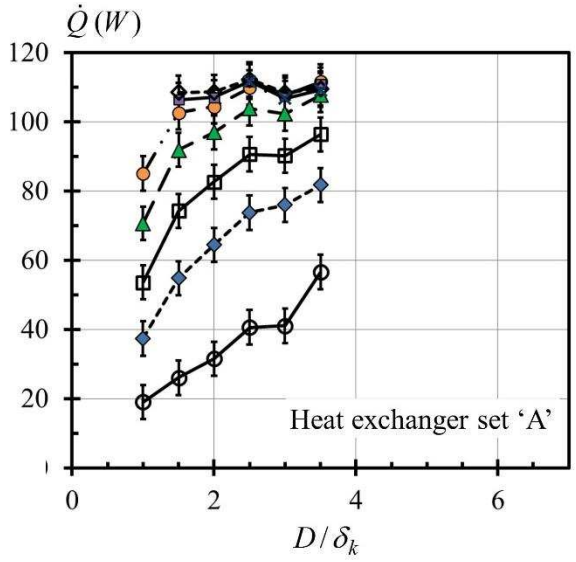

(a)

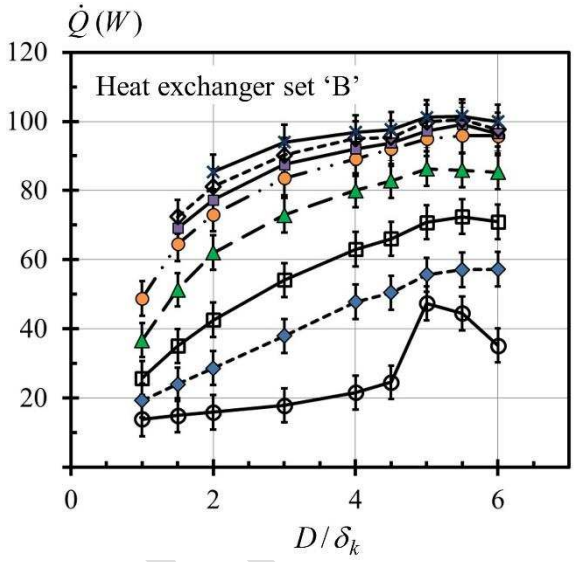

(b)

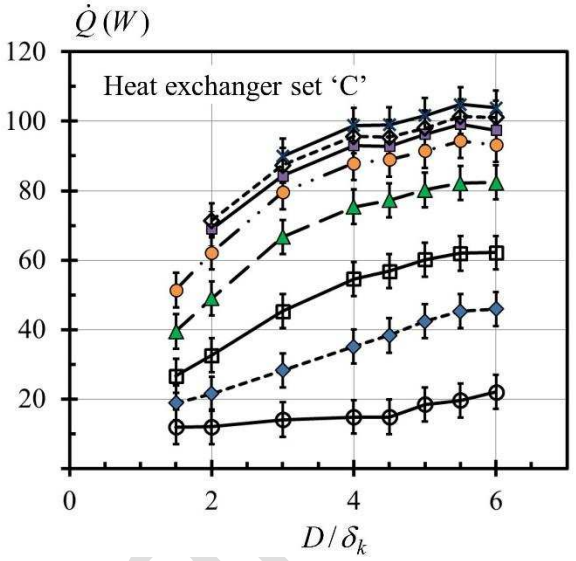

(c)

Legends	$(\xi_a - g)/(\sigma L)$		
	'A'	'B'	'C'
	0.7mmHEX	1.4mmHEX	2.1mmHEX
○	-0.04	-0.03	-0.03
◆	0.12	0.10	0.09
□	0.27	0.23	0.22
▲	0.59	0.50	0.47
●	1.06	0.91	0.85
■	1.37	1.17	1.11
◇	1.68	1.44	1.36
✕	2.15	1.84	1.74

Fig. 11: Dependence of $\dot{Q}$ on D/δ_k at various $(\xi_a - g)/(\sigma L)$ for $T_{h,i} = 80^oC$.

It can also be seen from Fig. 12(a) that the fin spacing influences the heat transfer coefficient: Colburn-j factor (j_{OSC}). In order to assist the design of thermoacoustic heat exchangers, a correlation to fit the experimental results is developed in the form $j_{osc} = aRe_1^m(t/D_h)^n$ where t is fin thickness. The coefficient a and the exponents m and n are obtained from data regression using non-linear curve fitting. The correlation, with the coefficient of determination (R^2) of 0.92, is obtained as

$$j_{osc} = 0.0313 Re_1^{-0.6394} (t/D_h)^{-1.2541}. \quad (29)$$

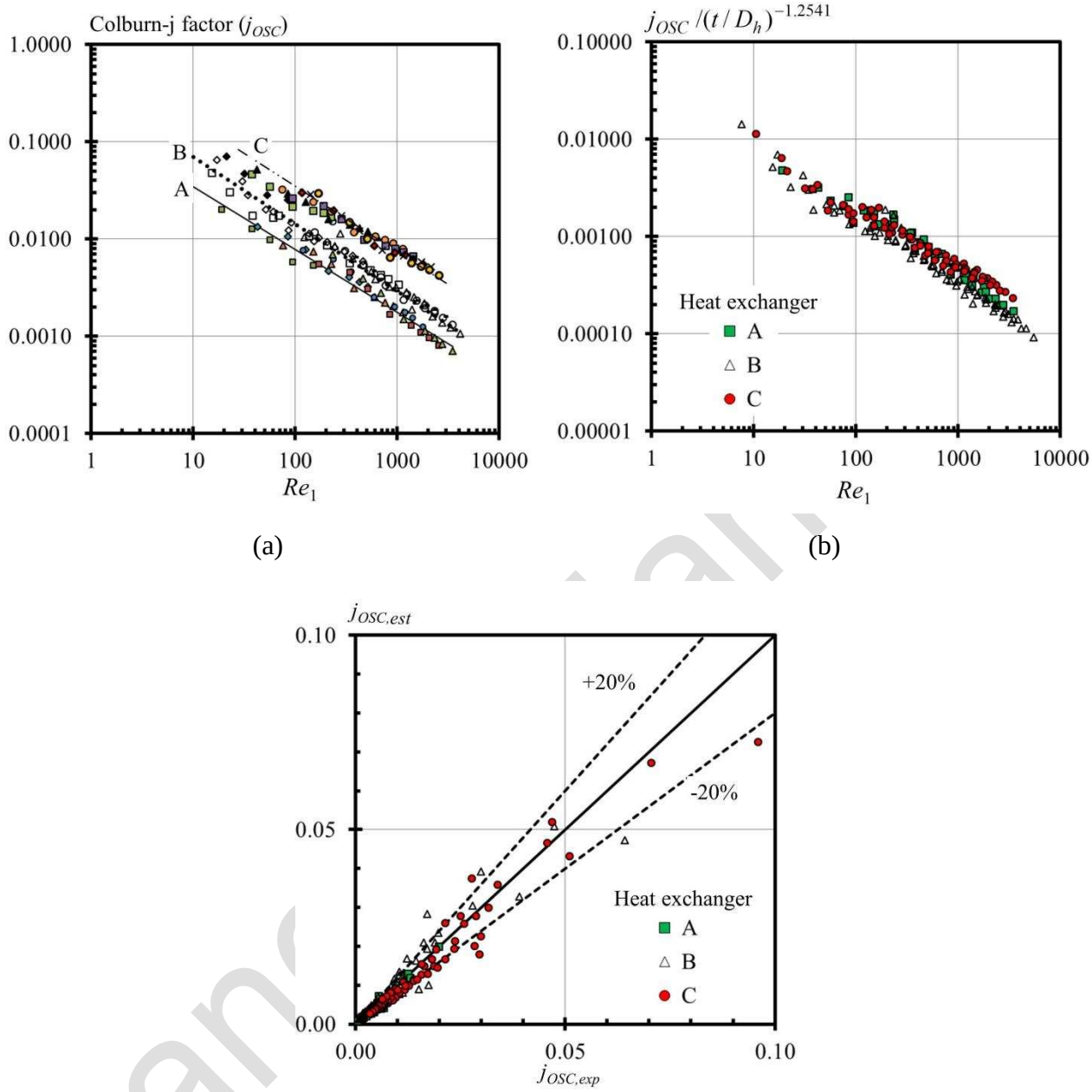

(a) (b)

(c)

Fig. 12: Measured gas side Colburn-j factor versus acoustic Reynolds number (Re_1) of three sets of heat exchanger plotted log-log scale (a), $j/(t/D_h)^{-1.2541}$ against Re_1 in log-log scale (b) and Colburn-j factor from experiment ($j_{OSC,exp}$) in comparison with the estimation ($j_{OSC,est}$) (c).

From the correlation and the results in Fig. 12(a), $j/(t/D_h)^{-1.2541}$ is plotted versus Re_1 in log-log scale in Fig. 12(b). The family of data points corresponding to different heat exchangers can be collapsed

to a group of points that fall close to a single line as shown. Thus, it is expected that the proposed correlation could help the design of finned-tube heat exchanger for oscillatory flow conditions. The comparison of the experimental Colburn-j factor ($j_{OSC,exp}$) and the estimated values ($j_{OSC,est}$) is also illustrated in Fig. 12(c) with the average deviation about 18%.

7. Conclusion

Heat exchangers are some of the most important components in thermoacoustic devices. The overall efficiency of such devices is greatly reliant on the heat transfer performance. However, the relationship between heat transfer and heat exchanger geometry and operating conditions is not well understood. The current study has developed experimental apparatus and techniques to investigate the heat transfer in oscillatory flows.

Steady flow experiment was carried out to get water side heat transfer coefficient (h_i) for facilitating the heat transfer analysis in oscillatory flow. In oscillatory flow experiment, heat transfer rates were calculated from the water side of the hot heat exchangers at various operating conditions. The influence of $(\xi_a - g)/(\sigma L)$ on $\dot{Q}$ was explored. For the heat exchanger set 'A', the values of $\dot{Q}$ increased rapidly for $(\xi_a - g)/(\sigma L) < 0.5$. The growth rate, however, was lower for the higher $(\xi_a - g)/(\sigma L)$ and almost levelled off when $(\xi_a - g)/(\sigma L) > 1.5$. A different trend was observed on the heat exchanger sets 'B' and 'C', where the values of $\dot{Q}$ continued to increase even when $(\xi_a - g)/(\sigma L) > 1.5$.

The effect of D/δ_k on $\dot{Q}$ was also determined. Generally speaking, $\dot{Q}$ increased with D/δ_k. For the heat exchanger sets 'B' and 'C', the maximum $\dot{Q}$ occurred at around $5.0 < D/\delta_k < 5.5$. Regarding heat exchanger set 'A', as the maximum D/δ_k in the experiment was at 3.5, the peak of $\dot{Q}$ was not clearly observed for $(\xi_a - g)/(\sigma L) < 1.06$. Nevertheless, it was expected that the peak of $\dot{Q}$ might appear at a higher D/δ_k, similar to heat exchanger sets 'B' and 'C'. Thus, it is likely that the optimal $\dot{Q}$ could be between $5.0 < D/\delta_k < 5.5$.

The heat transfer performance was also presented in dimensionless heat transfer coefficient: Colburn-j factor. The relationship between Colburn-j factor and acoustic Reynolds number (Re_1) was determined. A correlation for Colburn-j factor for each heat exchanger was developed. The average deviation between the Colburn-j factor from experiment ($j_{OSC,exp}$) and the estimation

($j_{OSC,est}$) is about 18%. The applicability of the proposed correlation to heat exchangers with different geometries and different working gases needs to be investigated further.

Acknowledgement

The project was financially supported by the EC-funded project "Thermoacoustic Technology for Energy Applications" under the 7th Framework Programme (Grant Agreement No. 226415, Thematic Priority: FP7-ENERGY-2008-FET, Acronym: THATEA). The funding enabled the development of the experimental apparatus and the necessary instrumentation. The first author also gratefully acknowledges the financial support received from the Royal Thai Government and the University of Phayao, Thailand.

References

1. Angell, C. A., M. Ogunl and W. J. Sichina (1982). "Heat capacity of water at extremes of supercooling and superheating." The Journal of Physical Chemistry **86**: 998-1002.
2. Archer, D. G. and R. W. Carter (2000). "Thermodynamic properties of the NaCl + H2O system. 4. Heat capacities of H2O and NaCl(aq) in cold-stable and supercooled states." The Journal of Physical Chemistry B **104**: 8563-8584.
3. Bouvier, P., P. Stouffs, et al. (2005). "Experimental study of heat transfer in oscillating flow." International Journal of Heat and Mass Transfer **48**(12): 2473-2482.
4. Brewster, J. R., R. Raspet, et al. (1997). "Temperature discontinuities between elements of thermoacoustic devices." Journal of the Acoustical Society of America **102**(6): 3355-3360.
5. British Standard Institution (1973). Methods for the Measurement of Fluid Flow in Pipes. Part 2. Pitot Tubes. England. **BS1042**.
6. Çengel, Y. A. (1997). Introduction to Thermodynamics and Heat Transfer. New York, McGraw-Hill.
7. Çengel, Y. A. and J. M. Cimbala (2006). Fluid Mechanics : Fundamentals and Applications. Boston, McGraw-Hill.
8. Coleman, H. W. and W. G. Steele (2009). Experimentation, validation, and uncertainty analysis for engineers. New Jersey, John Wiley & Sons.
9. Garrett, S. L., D. K. Perkins, et al. (1994). "Thermoacoustic Refrigerator Heat Exchangers - Design, Analysis and Fabrication." Heat Transfer 1994 - Proceedings of the Tenth International Heat Transfer Conference, Vol 4(135): 375-380.

10. Gust, J. C., R. M. Graham and M. A. Lombardi (2004). Stopwatch and Timer Calibrations. Washington, National Institute of Standards and Technology.
11. Incropera, F. P. (2006). Introduction to heat transfer. Chichester, Wiley.
12. Kim, J. H., T. W. Simon, et al. (1993). "Journal-of-Heat-Transfer Policy on Reporting Uncertainties in Experimental Measurements and Results." Journal of Heat Transfer – Transaction of ASME **115**(1): 5-6.
13. Kline, S. J. and F. A. McClintock (1953). "Describing Uncertainties in Single-Sample Experiments." Mechanical Engineering **75**(1): 3-8.
14. Klopfenstein, R. (1998). "Air velocity and flow measurement using a Pitot tube." ISA Transactions **37**: 257-263.
15. Mao, X. A., W. Kamsanam and A. J. Jaworski (2011). "Convective Heat Transfer from Fins-on-Tubes Heat Exchangers in an Oscillatory Flow." The 23rd IIR International Congress of Refrigeration.
16. Miller, V. (2002). Recommended guide for determining and reporting uncertainties for balances and scales. Washington, National Institute of Standards and Technology.
17. Mozurkewich, G. (2001). "Heat transfer from transverse tubes adjacent to a thermoacoustic stack." Journal of the Acoustical Society of America **110**(2): 841-847.
18. Nsofor, E. C., S. Celik, et al. (2007). "Experimental study on the heat transfer at the heat exchanger of the thermoacoustic refrigerating system." Applied Thermal Engineering **27**(14-15): 2435-2442.
19. Paek, I., J. E. Braun, et al. (2005). "Characterizing heat transfer coefficients for heat exchangers in standing wave thermoacoustic coolers." Journal of the Acoustical Society of America **118**(4): 2271-2280.
20. Rennels, D. C. and H. M. Hudson (2012). Pipe Flow : A Practical and Comprehensive Guide. Hoboken, New Jersey, Wiley.
21. Richardson, M. J. (02/12/2010) "Specific heat capacities." Accessed 02/05/2012 http://www.kayelaby.npl.co.uk/general_physics/2_3/2_3_6.html.
22. Robinson, R. A., D. Butterfield, et al. (2004). "Problems with Pitots issues with flow measurement in stacks." International Environmental Technology **1**.
23. Rood, E. P. and D. P. Telionis (1991). "Journal of Fluids Engineering Policy on Reporting Uncertainties in Experimental Measurements and Results." Journal of Fluids Engineering-Transactions of the Asme **113**(3): 313-314.
24. Seber, G. A. F., Wild, C. J., (2003). Nonlinear Regression. John Wiley & Sons, Inc.
25. Swift, G. W. (1988). "Thermoacoustic Engines." Journal of the Acoustical Society of America **84**(4): 1145-1180.

26. Swift, G. W. (2001). Thermoacoustics : a unifying perspective for some engines and refrigerators. Melville, NY, Acoustical Society of America through the American Institute of Physics.
27. Tang, K., J. Yu, et al. (2014). "Heat transfer of laminar oscillating flow in finned heat exchanger of pulse tube refrigerator." International Journal of Heat and Mass Transfer **70**: 811-818.
28. Wagner, W. and A. Prußb (2002). "The IAPWS formulation 1995 for the thermodynamic properties of ordinary water substance for general and scientific use." Journal of physical and chemical reference data **31**(2): 387-535.
29. Wakeland, R. S. and R. M. Keolian (2004). "Effectiveness of parallel-plate heat exchangers in thermoacoustic devices." Journal of the Acoustical Society of America **115**(6): 2873-2886.

Nomenclature

A_{min}	heat exchanger minimum air flow area (m^2)
A_f	fin surface area (m^2)
A_{fc}	fin cross sectional area (m^2)
$A_{t,i}$	water side heat transfer area (m^2)
A_o	gas side heat transfer area (m^2)
$A_{t,o}$	unfinned area on copper tube (m^2)
a	sound speed ($m{\cdot}s^{-1}$)
b	systematic uncertainty
c_p	isobaric specific heat ($kJ{\cdot}kg^{-1}{\cdot}K^{-1}$)
D	fin spacing (m)
D_h	fin spacing hydraulic diameter (m)
D_i	tube inside diameter (m)
D_o	tube outside diameter (m)
F	cross flow correction factor
f	frequency (Hz)
f_s	friction factor
g	half of the gap between hot and cold heat exchanger faces (mm)
HEX	hot heat exchanger
h	heat transfer coefficient ($W{\cdot}m^{-2}{\cdot}K^{-1}$)
j	Colburn-j factor
k	thermal conductivity ($W{\cdot}m^{-1}{\cdot}K^{-1}$)
k_w	wave number (m^{-1})
L	fin length (m)
L_c	corrected fin length (m)
L_T	effective length of copper tube (m)
LMTD	log-mean temperature difference (K)
$\dot{m}$	mass flow rate ($kg{\cdot}s^{-1}$)
Nu	Nusselt number
P_a	acoustic pressure amplitude (Pa)
Pr	Prandtl number
$\dot{Q}$	heat transfer rate (W)
R_{tube}	thermal resistance of tube material ($m^2{\cdot}K{\cdot}W^{-1}$)
Re	Reynolds number
Re_1	acoustic Reynolds number
r_1	inside radius of copper tube (m)
r_2	outside radius of copper tube (m)
s	precision uncertainty
T	temperature (^oC)
t	fin thickness (m)
u_1	velocity amplitude ($m{\cdot}s^{-1}$)
V	flow velocity ($m{\cdot}s^{-1}$)
Va	Valensi number
x	distance from pressure anti-node to heat exchanger (m)

Greek symbols

δ_k	thermal penetration depth (m)
ε_s	surface roughness (m)
η_f	single fin efficiency
η_o	overall fin efficiency
λ	wave length (m)
μ	dynamic viscosity ($Pa{\cdot}s$)
ξ_a	displacement amplitude (m)
Π	fin cross sectional perimeter (m)
ρ_m	mean density ($kg.m^{-3}$)
σ	heat exchanger porosity
ω	angular frequency ($rad{\cdot}s^{-1}$)

Subscripts

a	air
amb	ambient
avg	average
c	cold
est	estimation
exp	experiment
i	inlet
max	maximum
OSC	oscillatory flow
o	outlet
STD	steady flow
w	Water